Frequency-Domain Thermal Modeling of Power Modules Based on Heat Flow Spectrum Analysis

Mengqi Xu, Ke Ma, *Senior Member, IEEE*, Quan Zhong, and Marco Liserre, *Fellow, IEEE*

***Abstract*—Many efforts have been devoted to describe the multi-timescale thermal dynamics of power modules and frequency-domain modeling is a relatively new approach. Unfortunately, only the frequency-domain response of thermal impedance has been studied in recent works, so the existing models can only describe the temperature behaviors of semiconductors. In the reality, it is not only the temperature of semiconductors which is important but also of other parts of the package. In this article, a novel perspective to study the thermal dynamics by analyzing heat flow behaviors is proposed. Frequency spectrum analysis in finite-element method simulation has been first used in this article, and it reveals that heat flow of the power semiconductor device behaves as a multi-layer low-pass filter (LPF). As a result, a novel modelling method of heat flow with a 7order-3frequencies LPF has been developed in this article and it can provide a comprehensive description of heat flow behaviors for power modules at full bandwidth. Meanwhile, the effects on heat flow behaviors brought by boundary conditions are also considered to ensure that the proposed model can be easily adapted to different boundary conditions. The effectiveness and accuracy of the proposed model has been verified by both simulations and experiments.**

***Index Terms*—Curve fitting, finite-element method (FEM), frequency domain response, power modules, thermal modelling.**

I. Introduction

POWER semiconductor devices, especially insulated gate bipolar transistor (IGBT) modules, have been widely used in many important applications, such as renewable energy, aerospace, and electric vehicles, etc. Consequently, the reliability evaluation of the power modules is becoming an important research topic [1]. It has been widely accepted that thermal stress of power electronic devices including over-heat and thermal cycling, is one of the major causes of failures [2], there are strong demands for accurate prediction of the thermal dynamics of the power electronic devices under complex mission profiles.

Since the device loading contains various time constants from micro-seconds to years, the modeling of complete thermal behaviors in power modules is a very challenging task. In [3], three different modeling levels are separated according to the timescales of the interested thermal dynamics and their disturbances. But, the main problem of this approach is that many complex models at different physics domains are involved, and there is lack of connection among models at different timescales. Thereby, a method of handling multitime scale thermal dynamics of power device by frequency-domain analysis has emerged these days, and the frequency-domain response of thermal impedance becomes attractive.

There are primarily three methods for obtaining frequency-domain responses of device's thermal behaviors nowadays. One approach is to measure the transient thermal impedance and convert it to Foster or Cauer network, and then frequency domain representation can be acquired through time-frequency transformation. But, both of the thermal networks have their limitations: it is hard to obtain parameters of Cauer network because the physical structure/materials of the device should be provided [4] and Foster network cannot be directly connected with the thermal network outside device [5]. Furthermore, converting a thermal transient to a frequency domain representation is difficult because the conversion process is very sensitive to noise, especially at higher frequencies [6]. As a result, Wang and Qiao [7] proposes another approach to obtain frequency response by applying the fast Fourier transform to the time derivative of the transient thermal impedance, which removes the need of deriving an explicit expression of the system's transfer function. Another method of acquiring frequency-domain response is to excite the power devices with various losses at multiple frequencies over a wide bandwidth, so that the impedance response can be determined. In [8], [9], [10], [11], the thermal-impedance frequency response of power modules is extracted by *in situ* thermal impedance spectroscopy with small-signal loss excitation. In [12], the thermal impedance between pairs of devices is determined under the frequency-domain using a technique based on pseudorandom binary sequences.

Manuscript received 10 May 2022; revised 1 August 2022; accepted 21 September 2022. Date of publication 29 September 2022; date of current version 18 November 2022. This work was supported by National Nature Science Foundation of China under Grant 52177188. Recommended for publication by Associate Editor H. Peng. *(Corresponding author: Ke Ma.)*

Mengqi Xu is with the Key Laboratory of Control of Power Transmission and Conversion, Ministry of Education, Shanghai Jiao Tong University, Shanghai 200240, China (e-mail: mengqixu@sjtu.edu.cn).

Ke Ma is with the Department of Electrical Engineering, Shanghai Jiao Tong University, Shanghai 200240, China (e-mail: kema@sjtu.edu.cn).

Quan Zhong is with the Key Laboratory of Control of Power Transmission and Conversion, Ministry of Education, Shanghai Jiao Tong University, Shanghai 200240, China, and also with the Department of Electrical Engineering, Shanghai Jiao Tong University, Shanghai 200240, China (e-mail: zhongquan@sjtu.edu.cn).

Marco Liserre is with the Chair of Power Electronics, Christian-Albrechts University of Kiel, 24143 Kiel, Germany (e-mail: ml@tf.uni-kiel.de).

Color versions of one or more figures in this article are available at https://doi.org/10.1109/TPEL.2022.3210505.

Digital Object Identifier 10.1109/TPEL.2022.3210505

It can be concluded that many efforts have been paid to study the frequency-domain response of thermal impedance while the heat flow frequency response of power modules is seldom considered, but it has been proved that heat flow information is of great importance for thermal description of power moduless [13]. In 2016, it was discovered that the gain of heat flow from $P_{\rm in}$ (injected power-loss/heat into device) to $P_{\rm out}$ (heat flowing out of device) behaves as a low-pass filter (LPF) under frequency domain as shown in [14], so that LPF was first proposed to describe the heat flow characteristics of power device. However, the structure of LPF was not defined clearly in this article, which used a multilayer Cauer thermal network as reference. Although the Cauer thermal network can represent power device thermal transients, it is difficult to assure the correctness of frequency-domain responses since the time-frequency conversion process is very sensitive to noise [6]. Furthermore, the multilayer LPF in [14] was degraded to three cascaded LPFs at first-order for simplification and too much information was ignored. Thus, the LPF has systematic deviations in various frequency bands, proving that the existing structure of LPF is not accurate enough.

In this article, the heat flow spectrum in frequency domain is first studied in FEM simulations and then an advanced frequency-domain thermal model with a 7order-3frequencies LPF for power modules is proposed. The structure of the proposed LPF is carefully considered based on the simulated results by frequency spectrum analysis of heat flow behaviors in FEM simulation and its derivation process is provided in detail. Compared with existing models as Foster and Cauer, the proposed modeling method can provide a comprehensive description of heat flow behaviors for power modules at full bandwidth and the characterization method is relatively simple that only external measurement is needed without knowing physical structure/materials inside the device. In Section II, the modeling method based on thermal spectrum analysis with FEM simulation will be introduced and simulation verification will be provided. In Section III, the impacts of boundary conditions on the heat flow behaviors will be explained in frequency domain and the changes on model parameters will also be introduced. In Section IV, the proposed modeling method will be verified by experiments.

II. Thermal Spectrum Analysis With FEM Simulation and Proposed Heat Flow Modeling Method

A. Problems of Existing LPF Structure for Heat Flow

The existing LPF in [14] is proposed based on the analysis of the seven-layer Cauer model, whose thermal resistance and thermal capacitance may be simply calculated as follow if a heat spreading angle of 45° is assumed [15], [16]

$$R_{th} = \frac{d}{kS} \tag{1}$$

$$C_{th} = V \rho c_p \tag{2}$$

where *d, k, ρ, c, V*, and *S* represent the material thickness, thermal conductivity, material density, specific heat capacity, effective area and volume, respectively.

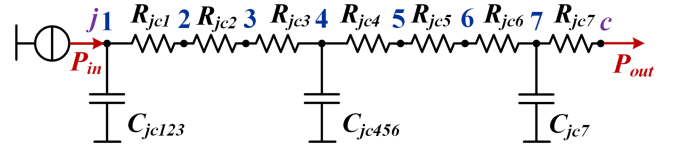

Fig. 1. LPF structure from the seven-layer Cauer for reference in [14].

Although the heat spread angle in different material is considered in some studies [16], [17], [18], [19], the accuracy of the frequency-domain characteristics of this seven-layer Cauer cannot be guaranteed. As stated in [19], the calculation of the parameters of this seven-layer Cauer model is based on some ideal assumptions, e.g., the thermal resistance has to be calculated between isothermal surfaces and the heat that flows into the first surface has to flow out through the second. Therefore, this seven-layer Cauer model is not accurate enough to be set as reference. Another cause of the inaccurate estimation for thermal behaviors of power semiconductor device by using the existing method in [14] is that the degradation method of simplification for LPF is applied. To be specific, the seven cascaded LPFs are degraded into three cascaded LPFs at first-order as shown in Fig. 1. Therefore, the transfer function for the heat or power loss from input to output of the device $G_{P{\rm in}\,P{\rm out}}\,(s)$ is estimated as the heat gain $G_{\rm LPF}\,(s)$ in existing works

$$\begin{aligned} G_{P_{\rm in}P_{\rm out}}\,(s) &\approx G_{\rm LPF}\,(s) \\ &= \tfrac{2\pi f_{cr1}}{s+2\pi f_{cr1}} \cdot \tfrac{2\pi f_{cr2}}{s+2\pi f_{cr2}} \cdot \tfrac{2\pi f_{cr3}}{s+2\pi f_{cr3}} \end{aligned} \tag{3}$$

where f_{cr1}, f_{cr2}, and f_{cr3} are the critical frequencies of the simplified LPF, and *s* is the Laplace operator. The order of the LPF is thereby reduced to three by using this method and it is inevitable that the thermal behaviors in some frequency bands will be ignored during curve fitting process for characterizing the parameters. Thus, it is almost impossible to eliminate this deviation if this simplification method for LPF is applied.

B. Thermal Spectrum Analysis With FEM Simulations

As mentioned above, the seven-layer Cauer model may not be able to provide reliable references for frequency-domain thermal analysis. Therefore, this article first builds a FEM model in COMSOL, and then conducts frequency-domain thermal simulations to get more reliable results. A 650V/50A power IGBT module with six IGBTs and six diodes is studied in this article. The parameters for the material of each layer of the IGBT module are given in Table I and the construction of the studied IGBT module for FEM simulation is illustrated in Fig. 2. The total mesh has 103 269 domain elements, 40 518 boundary elements and 4794 edge elements. As for the cooling system outside the IGBT module, equivalent heat transfer coefficient (htc) is often used as a simplified thermal boundary condition to indicate the heat dissipation capability of the cooling system in many literatures [20]. For different cooling systems, htc varies from 10 W/m^2·K to 10^5 W/m^2·K [21] and htc = 3000 W/m^2·K is picked as a reference in this article. It should be noted that this article only focuses on the thermal behavior of single IGBT device under test (DUT) as marked in Fig. 2, and that the thermal

TABLE I
PARAMETERS FOR THE MATERIAL OF IGBT MODULE

Layers	Material	Thickness d (mm)	Density ρ (kg/m^3)	Thermal conductivity λ (W/m·K)	Specific heat C_p (J/kg·K)
Chip	Si	0.13	2330	148	710
Chip Solder	Sn-3.5Ag-0.5Cu	0.08	7500	33	230
Copper	Copper	0.3	8700	395	385
DCB	Al_2O_3	0.38	3750	24	896
Copper	Copper	0.3	8700	395	385
Baseplate Solder	Sn-3.5Ag-0.5Cu	0.2	7500	33	230
Baseplate	Copper	3	8700	395	385

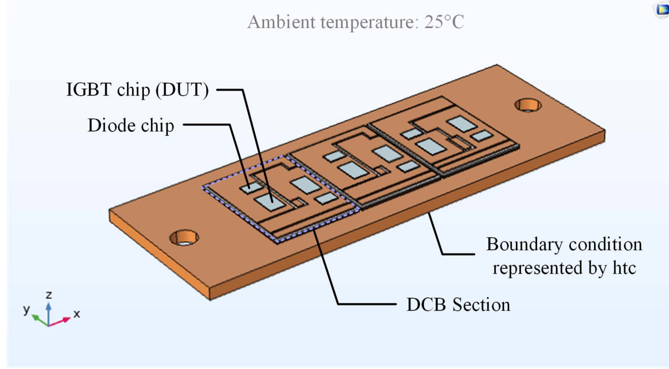

Fig. 2. Construction of the studied IGBT module modeled in COMSOL for FEM analysis.

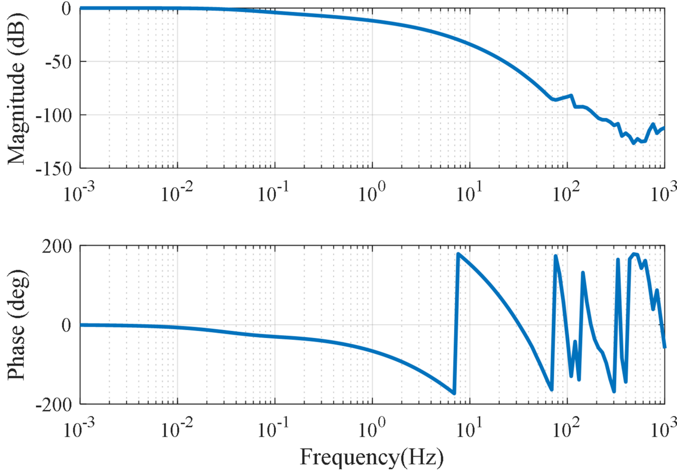

Fig. 3. Bode plot of the heat gain from input loss to output by FEM simulation.

coupling effect between adjacent chips will be investigated in further research.

For FEM thermal simulation, the heat transfer in solids module in COMSOL needs to be activated first. There are two steps to obtain thermal spectrum of DUT in frequency domain: the first step is a Stationary study step which computes the stationary/bias solution; the second step is the frequency domain perturbation step, which computes a perturbed solution of the linearized problem around the linearization point (or bias point) computed in the first step [22]. As a result, the bode plot of the heat gain from input loss to output $G_{Pin\,Pout}(s)$ can be obtained, as shown in Fig. 3, proving that heat flow indeed behaves like a LPF and the remaining issue is the structure of LPF.

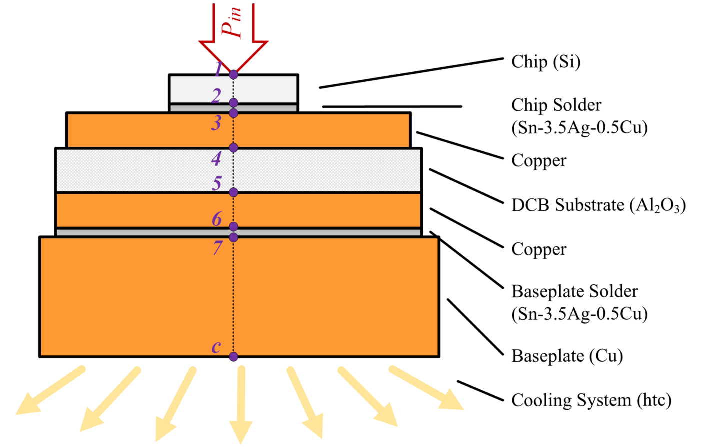

Fig. 4. Locations of the point probes for heat flow of DUT during FEM simulation.

C. Modelling Method With Proposed 7order-3frequencies LPF

The existing LPF in [14] is constructed based on the classification of three groups according to the magnitude of cumulative gains of heat flow $|G_{P_{in}P_n}(s)|$, where n corresponds the nodes in Fig. 1. Here, another method of classification based on heat flow spectrum from FEM simulations by observing the gains of heat flow between the two adjacent nodes $|G_{P_nP_{n+1}}(s)|$ instead of the cumulative heat gains is proposed. Similarly, the main purpose is to reduce the undetermined parameters (critical frequencies in LPF) from seven to three, corresponding to the three frequency bands/ timescales as described in [1] and [23]. The specific locations of measured points for heat flow nodes are located on the surface of each layer, where the measuring point for the junction node is in the center of the DUT and all the points are allied in the same vertical line as shown in Fig. 4. It should be mentioned that point probes are applied in this simulation to provide the value of heat flux field quantity at these specific points.

In this study case, the magnitude of gains of heat flow between the two adjacent nodes in frequency domain from heat flow spectrum is illustrated Fig. 5. It should be noted that the frequency-domain characteristics of the module correlate closely with the materials and it would be too complicated if the structure of filter for each layer is carefully considered. Therefore, the gains of heat flow between the two adjacent nodes $|G_{P_nP_{n+1}}(s)|$ can be treated as first-order LPFs for convenience. As for filters, the -3 dB point is very commonly used, representing the filter cuts

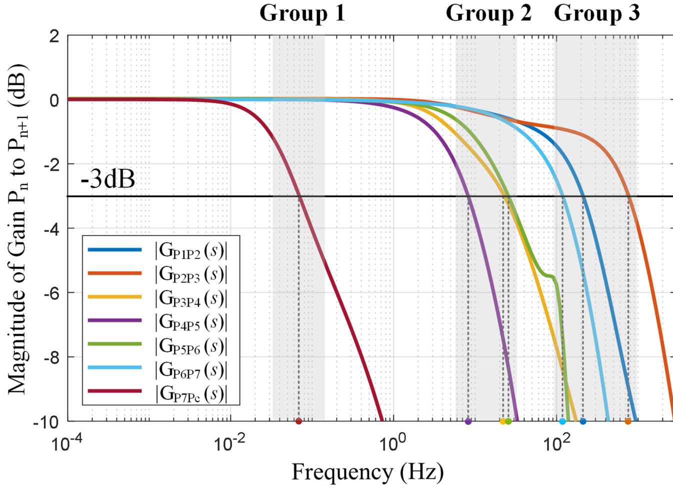

Fig. 5. Proposed classification method based on magnitude of gains of heat flow between two adjacent nodes in frequency domain when the baseplate with htc = 3000 W/m^2·K of lower surface is considered.

off half of the power at that frequency. Thereby, it is applied here to construct the structure of LPF for describing heat flow behaviors.

Since the corresponding frequency of $G_{P_7P_c}(s)$ (the baseplate layer) at -3 dB is much lower than the others, the baseplate layer is divided into group 1 alone. As for $G_{P_4P_5}(s)$ (the DCB layer), the corresponding frequency at -3 dB is close to $G_{P_3P_4}(s)$ and $G_{P_5P_6}(s)$ (the copper layers), so they can be classified into the same group named group 2. As a matter of fact, the corresponding frequency of $G_{P_2P_3}(s)$ (the chip solder layer) is around 1 kHz, which is almost impossible to be detected by means of existing thermal measurements, such as optical fiber temperature sensors (around 30 Hz). Therefore, the chip solder layer, the chip layer and the baseplate solder layer can be classified into the same group named group 3 as shown in Fig. 5.

Then, a novel LPF based on the grouping result without reducing the order is proposed and the expression is presented as

$$G_{\text{LPF}}^{\text{New}}(s) \approx \left(\frac{2\pi f_1}{s+2\pi f_1}\right)^1 \left(\frac{2\pi f_2}{s+2\pi f_2}\right)^3 \left(\frac{2\pi f_3}{s+2\pi f_3}\right)^3 \quad (4)$$

where $f_1 < f_2 < f_3$, and s is the Laplace operator.

The proposed simplified LPF is a seventh-order low pass filter and the frequency band is divided into three parts and each parameter in this LPF has its explicit mathematical and physical meaning: f_1 corresponds to low frequency band; f_2 corresponds to medium frequency band; and f_3 corresponds to high frequency band. For example, f_3 corresponds to high frequency band which is composed of chip layer, chip solder layer and baseplate solder layer of the studied device. If f_3 changed significantly after a long-time operation, this may be an indicator that degradation might already happened in these regions. On the other hand, the structure of LPF for different power modules can be different, but it is convenient to determine the structure of LPF for each specific device by using the proposed method.

Thereby a novel frequency-domain thermal model with the novel simplified LPF is proposed. In this model, the structure of the LPF is clearly defined, which is a seventh-order low pass filter with three critical frequencies as illustrated in Fig. 6 and the transfer function of LPF is represented in (4).

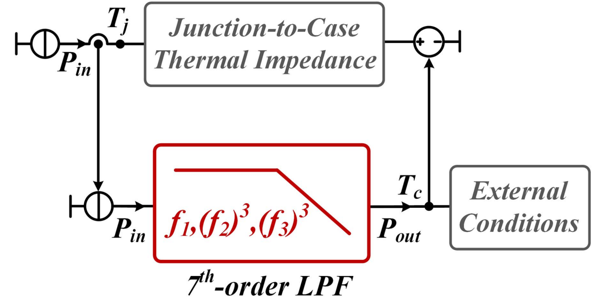

Fig. 6. Proposed frequency-domain thermal model with a 7order-3frequencies LPF for power modules.

D. Characterization Method and Simulation Verification

The junction-to-case thermal impedance in this proposed model can be either Foster or Cauer network, and it can be characterized by time-domain curve fitting. Therefore, the main problem is the characterization of LPF and external conditions in proposed model.

As for the LPF, P_{in} is the input of heat source/power loss generated on the chip and is defined as a step signal in the time domain during characterization process. Therefore, the frequency domain expression of P_{in} can be represented as

$$P_{\text{in}}(s) = \frac{P_{\text{in}}}{s}. \quad (5)$$

So the output heat flow $P_{\text{out}}(s)$ can be calculated as

$$P_{\text{out}}(s) = P_{\text{in}}(s) \cdot G_{P_{\text{in}}P_{\text{out}}}(s) \approx P_{\text{in}}(s) \cdot G_{\text{LPF}}^{\text{New}}(s). \quad (6)$$

By applying inverse Laplace transform, to (6), time-domain heat flow $P_{\text{out}}(t)$ can be represented as

$$P_{\text{out}}(t) = \mathcal{L}^{-1}\{P_{\text{out}}(s)\}. \quad (7)$$

As a result, the critical frequencies of proposed LPF in (4) can be characterized by mathematical fitting from $P_{\text{out}}(t)$ curve using the expression of (7). The time-domain plots of the predicted heat flow by using the expression of (7) is shown in Fig. 7, which have a good agreement with the FEM simulation compared with the existing methods, including Foster network fitted from transient thermal impedance, and Cauer network calculated by (1), (2). It is worth noting that the results of Foster model in Fig. 7 are added only for completeness but they have no physical meaning. The three frequencies of the proposed method in green are identified as $f_1 = 0.2235$, $f_2 = 16.5$, and $f_3 = 81.39$ Hz, respectively, and the time-domain simulated results show that the accuracy of the heat flow predictions can be improved to 0.01 s by using this proposed method. Furthermore, the ripples appear in Fig. 7 because of the intrinsic problem of time-dependent solver algorithm in COMSOL. Time-dependent solver is used in COMSOL to find the solution to dynamic problems and it offers three different time stepping methods: The implicit BDF and Generalized alpha methods and the explicit Runge–Kutta methods. The Runge–Kutta is appropriate for systems of

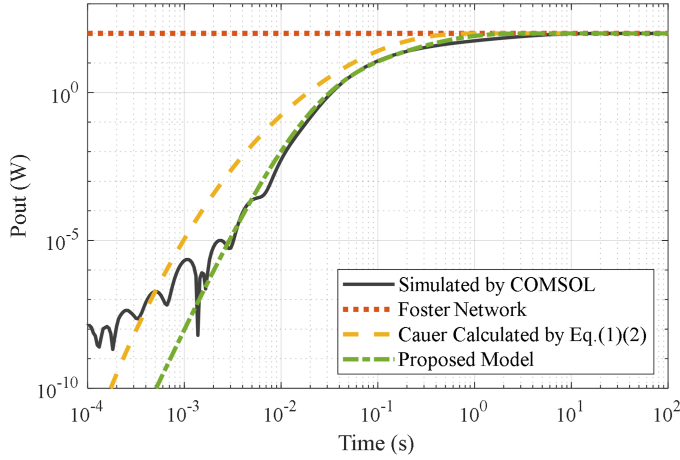

Fig. 7. Simulated comparison of time domain response of heat flow by proposed LPF and existing methods.

ordinary differential equations and are usually not as efficient for problems involving partial differential equations. Thereby, only BDF and generalized alpha can be applied in this case but both of the two methods have severe damping effects, especially the lower order BDF [24]. Fortunately, the ripples are ignorable that the maximum value is less than 10^{-5} and they only happen before 10^{-2} s, so that it has little effect on temperature calculation.

To represent the capability of the cooling system, the equivalent htc of the cooling system is used in FEM simulations but it is difficult to be applied in the proposed model. Thereby, the modeling of external conditions should also be carefully considered. As shown in Fig. 6, the input of external conditions in the proposed model is the output of LPF P_{out}, so that the temperature difference happened on the case should be calculated by

$$\Delta T_{ca}\left(s\right) = P_{\text{out}}\left(s\right).Z_{th(c-a)}\left(s\right) \quad (8)$$

where a refers to ambient node and the ambient temperature Ta equals to 25 °C here. If three-layer Foster network is applied for the external cooling condition, so its frequency-domain expression can be represented as

$$Z_{th(c-a)}\left(s\right) = \sum_{i=1}^{3} \frac{R_i}{R_i C_i \cdot s + 1}. \quad (9)$$

Since the time-domain step response of case temperature can be obtained by transient simulation, the RC parameters of $Z_{th(c-a)}$ can be determined by fitting the expression of inverse Laplace transformed (8) as

$$\Delta T_{ca}\left(t\right) = \mathcal{L}^{-1}\left\{P_{\text{in}}\left(s\right) \cdot G_{\text{LPF}}^{\text{New}}\left(s\right) \cdot Z_{th(c-a)}\left(s\right)\right\}. \quad (10)$$

Then, the thermal impedance of cooling system can be obtained, and the fitted result is given in Table II.

As a result, the junction and case temperatures when injecting 100 W step power loss into the IGBT chip predicted by different models are shown in Fig. 8, where the proposed model has a good agreement with simulated results. It can be seen that both the Foster network and Cauer network are unable to provide accurate estimation for thermal dynamics with the identified thermal impedance of cooling system from Table II. Therefore, both

TABLE II
IDENTIFIED FOSTER-TYPE THERMAL IMPEDANCE OF COOLING SYSTEM BY PROPOSED METHOD

Thermal Resistance $R_{1\text{-}3}$ (K/W)	Thermal Capacitance $C_{1\text{-}3}$ (J/K)
0.09985	0.01
0.09982	0.01
0.08965	60.82

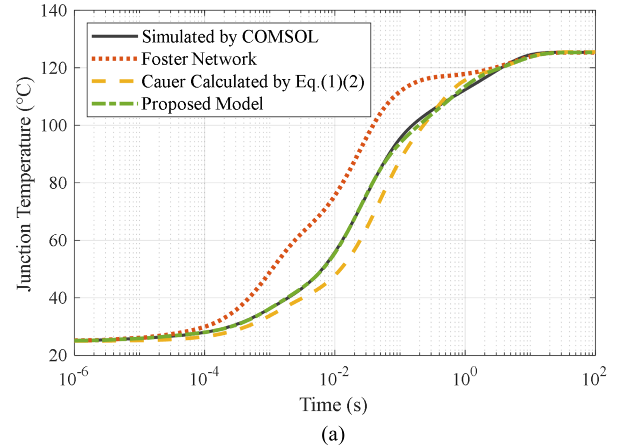

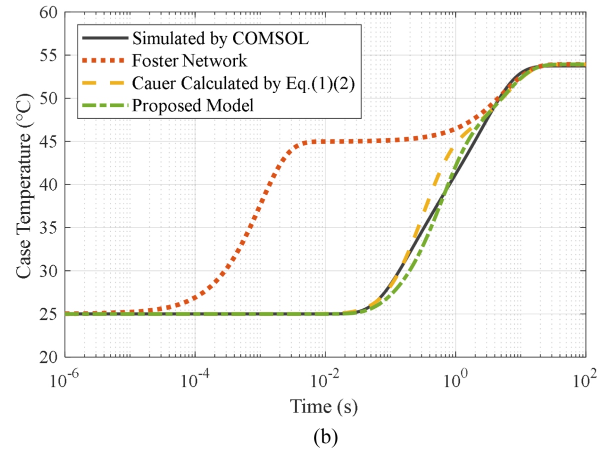

Fig. 8. Simulated comparison of time domain response of temperature by proposed LPF and existing methods. (a) Junction temperature. (b) Case temperature.

the widely used thermal networks have significant limitations on predicting thermal behaviors while the proposed model can provide a comprehensive description of thermal dynamics for power modules, including temperature and heat flow characteristics.

III. IMPACTS OF BOUNDARY CONDITIONS ON THE MODEL PARAMETERS

Similar to thermal impedance, the boundary conditions also have an effect on heat flow behaviors. To comprehend the significance of boundary condition effects on the heat flow of an IGBT module, cooling system variations and power loss variations are considered by frequency-domain FEM simulations, and the LPF parameters are characterized using the aforementioned method.

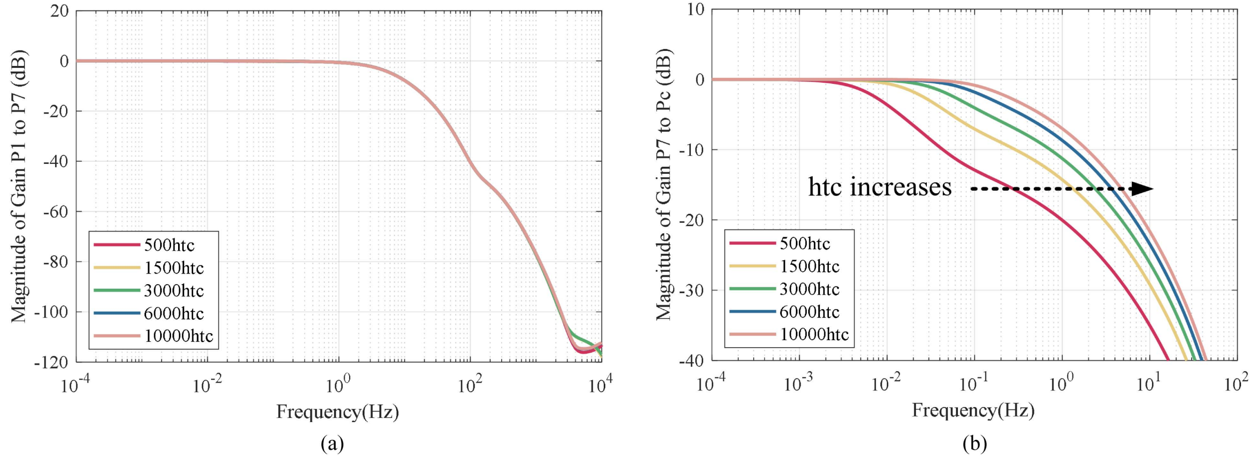

Fig. 9. Magnitude of gains of heat flow with htc varying from 500 to 10 000 W/m^2·K. (a) $G_{P_1P_7}(s)$. (b) $G_{P_7P_c}(s)$.

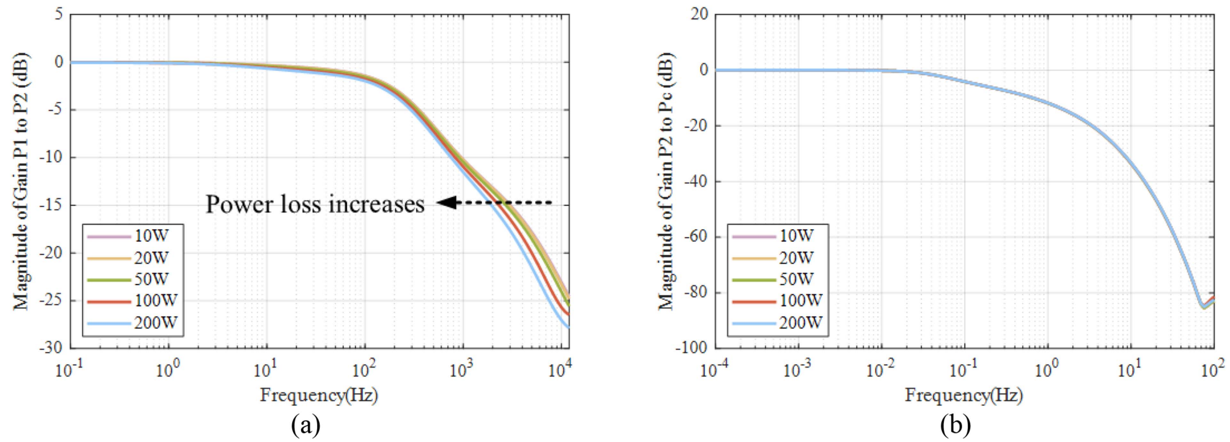

Fig. 10. Magnitude of gains of heat flow with input power loss varying from 10 to 200 W. (a) $G_{P_1P_2}(s)$. (b) $G_{P_2P_c}(s)$.

A. Variation of Cooling System

As stated in [21], htc varies from varies from 10 W/m^2·K to 10^5 W/m^2·K depending on the cooling mechanism. In this article, the htcs in the range of 500 to 10 000 W/m^2·K are used, which are reasonable values for the IGBT module's cooling system. As illustrated in Fig. 9, the magnitude of $G_{P_7P_c}(s)$ significantly changes according to the cooling system variation while the magnitude of $G_{P_1P_7}(s)$ remains unchanged. As a result, only the parameter of lowest frequency f_1 in proposed LPF will be influenced under this circumstance and its changing trend is plotted in Fig. 11(a). The corresponding polynomial fitting coefficients are also given and R^2 represents the coefficient of determination in statistics, which is a goodness-of-fit measure range from zero to one.

B. Variation of Power Loss

In this circumstance, the htc is set to 3000 W/m^2·K, and the IGBT chip is excited with different step power losses to investigate the impact of heat sources on the heat flow behaviors. According to the datasheet of this studied 650 V/50 A power IGBT module, the step power losses vary from 10 to 200 W. As shown in Fig. 10, the magnitude of $G_{P_1P_2}(s)$ changes according to the power loss variation, whereas the magnitude of $G_{P_2P_c}(s)$ remains unchanged. As a result, only the parameter of highest frequency f_3 in proposed LPF will be influenced under this circumstance and its changing trend with polynomial fitting coefficients is plotted in Fig. 11(b).

IV. Experimental Validations

To verify the proposed modeling method, the same 650 V/50 A IGBT power module is taken as an example for experimental tests. The temperatures are measured by T-type thermocouples (omega TJC36-CPSS-020G-2) and connected to the ten-channel HIOKI LR8432 Heat Flow Logger. During the experimental process, only one chip of the module is heated and the temperature probes are placed right beneath the heated IGBT chip.

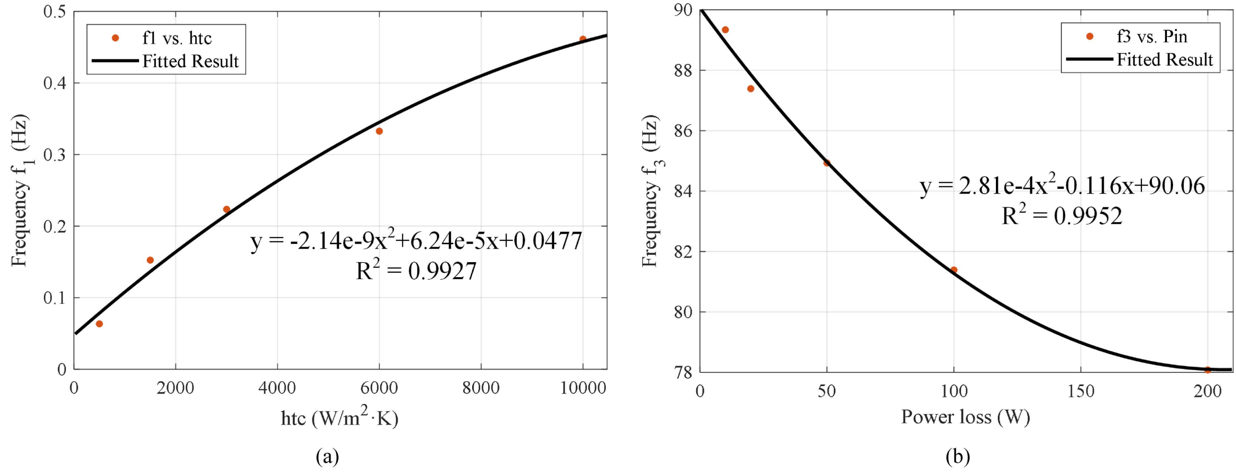

Fig. 11. Impacts of boundary conditions on model parameter (a) Changing trend of f_1 depending on the cooling system variation and its polynomial fitting. (b) Changing trend of f_3 depending on the power loss variation and its polynomial fitting.

A. Limitations of Heat Flow Measurement and Proposed Solutions

In the proposed method, the main idea is to characterize frequencies of the proposed LPF from P_{out} curve, which is difficult to be directly measured. As a result, the method of obtaining the heat flow behavior P_{out} (t) by indirect approach through two temperature nodes is adopted as follows:

$$P_{\text{out}}\ (t) = \frac{T_c\,(t) - T_h\,(t)}{Z_{ch}}\ . \tag{11}$$

However, $Z_{ch}(t)$is impossible to define without precise measurement of P_{out} (t), which creates a paradox. As a matter of fact, the thermal capacitance C_{th} of thermal grease is usually smaller than 1 (*J/K*) because the thickness of thermal grease is usually less than 100 μm when device is well installed on the cooling system. Therefore, (11) can be simplified as (12) to estimate P_{out} (t) by supposing only pure thermal resistance exists in the layer of thermal grease, if the two temperature sensors are close enough

$$P_{\text{out}}\,(t) \approx \frac{T_c\,(t) - T_h\,(t)}{R_{ch}}. \tag{12}$$

The difference of obtained P_{out} (t) curve by using different probes is carefully studied by FEM simulations. In order to demonstrate the influence caused by the distance, a thermal grease layer is added during FEM simulations with the temperature probe for case on the upper surface and the temperature probe for heatsink on the lower surface. Since only thermal resistance is considered in this case, the specific heat C_p of the material for thermal grease is set as zero and the difference of obtained P_{out} (t) curve by using different probes is demonstrated by adjusting the thickness of this layer as shown in Fig. 12. It can be concluded that the greater the distance, the error caused by this measurement method is larger. Fig. 12 also illustrates that the measured thermal resistance R_{ch} in this experiment is recommended to control within 0.15 K/W.

Another problem is the limitation of sensors. Although the temperature sensors applied in the setup are claimed to have a

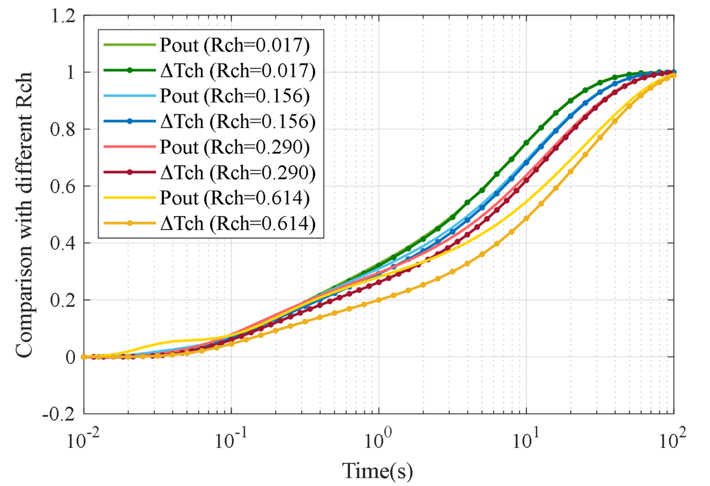

Fig. 12. Comparison of obtained P_{out} (t) curve by using temperature probes with different R_{ch} in FEM simulation.

measurement range of −200 °C to 700 °C with the accuracy of ±1 °C and the response time of 0.1 s, the influence on the measured P_{out} (t) cannot be ignored. It is difficult to further improve the accuracy of sensors, but there is one way to minimize the effects brought by the response time. In (13), τ is defined as the time constant of the delay block, which is the time in seconds the sensors need to respond to 63% of the step-change in temperature

$$G_{\text{delay}}\ (s) = \frac{1}{\tau \cdot s + 1}\ . \tag{13}$$

Therefore, the output heat flow P_{out} (s) should be modified as

$$\begin{aligned} P_{\text{out}}^{\text{exp}}\ (s) &= \tfrac{G_{\text{delay}}(s)\cdot T_c(s) - G_{\text{delay}}(s)\cdot T_h(s)}{R_{\text{ch}}} \\ &= G_{\text{delay}}\ (s) \cdot P_{\text{out}}\ (s) \end{aligned}\ . \tag{14}$$

By combining (6) and (14), the experimental time-domain output heat flow can be obtained by using inverse Laplace

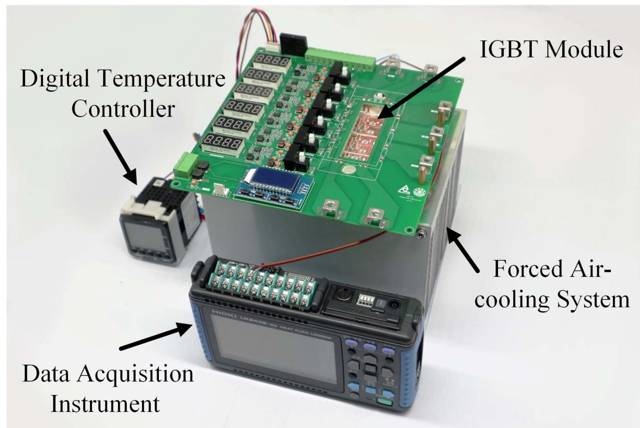

Fig. 13. Experimental setup for thermal characterization of the IGBT module.

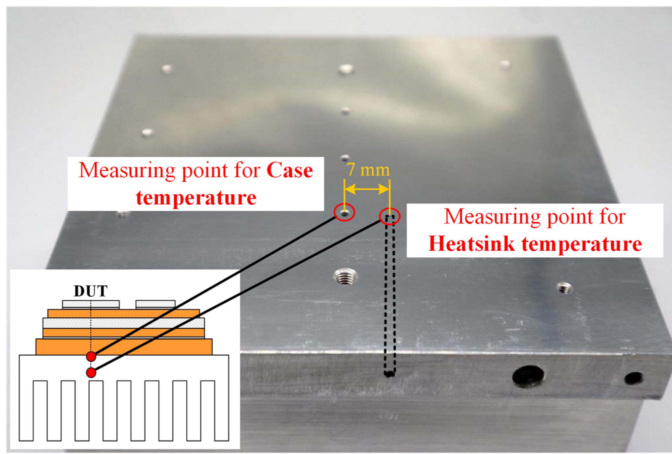

Fig. 14. Customized heatsink with mounting holes for case and heatsink temperature sensors.

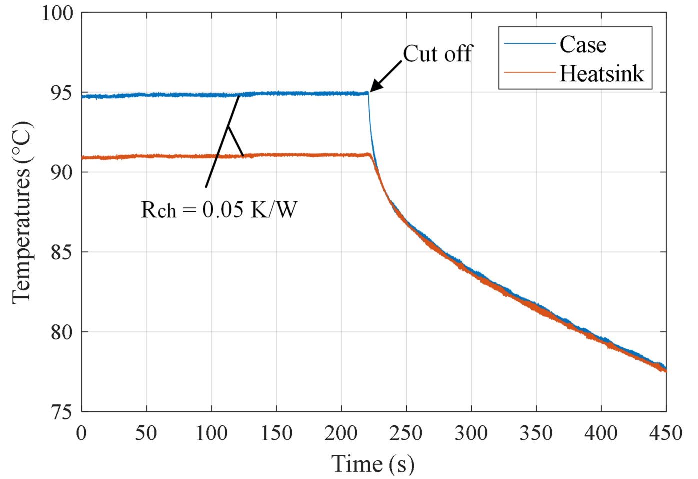

Fig. 15. Recorded temperature curves for case and heat sink under a step power loss of 73.8 W.

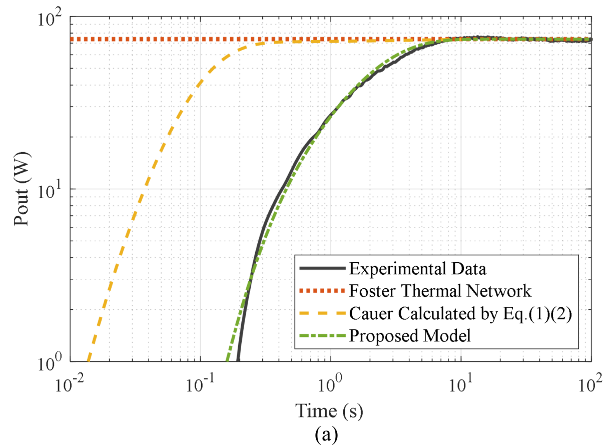

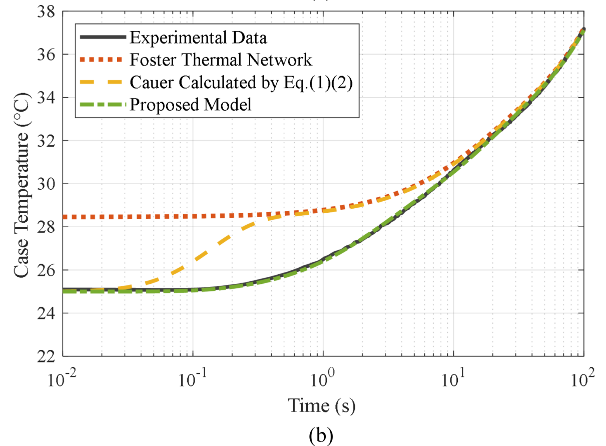

Fig. 16. Experimental comparison of thermal behaviors predicted by the proposed method with existing methods. (a) Heat flow. (b) Case temperature.

transform and the detailed expression can be obtained by running several lines of code in MATLAB.

B. Experimental Results

The experimental setup is shown in Fig. 13 and a 650 V/50 A IGBT power module is applied in this article. As mentioned in above, the measuring points for case and heatsink node should be set very close to each other to reduce measurement error, the distance between the two nodes here is 7 mm and the mounting locations of temperature sensors are depicted in Fig. 14. According to the JEDEC Standard [25] and Infineon application note [26], the temperature curves should be measured during turn-OFF process and the recorded temperature curves need to be vertically mirrored. Before cutting off the current, the chip is heated with constant current 45 A and conduction voltage of 1.64 V, which is equivalent to a step power-loss of 73.8 W. The experimental curves of case and heat sink under a step power loss of 73.8 W are shown in Fig. 15, which indicates that R_{ch} equals to 0.05 K/W, much smaller than the recommended 0.15 K/W as stated in Section A.

Thereby, the $P_{\mathrm{out}}\ (t)$ curve can be obtained by using (12) and the parameters are identified by proposed method. Considering that f_3 may be hard to identify because the response time of thermocouples is limited to 0.1 s, the lower bound of f_3 is set to 100 Hz to reduce the influence on the accuracy of f_1 and f_2 brought by the uncertainty of f_3. As a result, the three frequencies

of the proposed method by experiment are identified as $f_1 = 0.086$, $f_2 = 5.684$, and $f_3 = 109.82$ Hz respectively.

The comparison of time-domain step response of thermal behaviors with proposed model and existing models is plotted in Fig. 16, which directly shows that the proposed model with identified parameters has a good agreement with the experiments compared with existing and both the heat flow and temperature characteristics of the studied IGBT chip can be perfectly described by the proposed model. Another advantage of this method is that the characterization of the proposed thermal model is much easier when ensuring the accuracy of results. Only two temperatures outside the module (case and heatsink) should be measured in the proposed method while junction and case are need to be measured simultaneously in most existing methods. It is well known that junction temperature is difficult and complicated to measure in some cases. Thus, this proposed frequency-domain thermal model provides possibility for characterizing the heat flow behaviors inside without decapsulation of the power module.

V. Conclusion

This article presents a novel thermal modeling method for power modules. Different from existing methods, heat flow spectrum of IGBT chip in frequency domain has been first studied in FEM simulations and an advanced frequency-domain thermal model with a 7order-3frequencies LPF has been presented. There are three parameters (f_1, f_2, and f_3) in the proposed LPF and the derivation process of this special structure has been explained in detail. The effectiveness of this proposed frequency-domain thermal model has been verified by FEM simulations and experiments. Also, this article studies the boundary condition effects on the heat flow of a power module, which uncovers that the power loss variations mainly influence f_3 (high frequency band) of the LPF while the cooling system variations mainly influence f_1 (low frequency band) of the LPF.

References

[1] K. Ma, H. Wang, and F. Blaabjerg, “New approaches to reliability assessment: Using physics-of-failure for prediction and design in power electronics systems,” *IEEE Power Electron. Mag.*, vol. 3, no. 4, pp. 28–41, Dec. 2016.

[2] V. Smet et al., “Ageing and failure modes of IGBT modules in high-temperature power cycling,” *IEEE Trans. Ind. Electron.*, vol. 58, no. 10, pp. 4931–4941, Oct. 2011.

[3] K. Ma and F. Blaabjerg, “Multi-timescale modelling for the loading behaviours of power electronics converter,” in *Proc. IEEE Energy Convers. Congr. Expo.*, 2015, pp. 5749–5756.

[4] J. Li, A. Castellazzi, M. A. Eleffendi, E. Gurpinar, C. M. Johnson, and L. Mills, “A physical RC network model for electrothermal analysis of a multichip SiC power module,” *IEEE Trans. Power Electron.*, vol. 33, no. 3, pp. 2494–2508, Mar. 2018.

[5] M. Xu, K. Ma, B. Liu, and X. Cai, “Modeling and correlation of two thermal paths in frequency-domain thermal impedance model of power module,” *IEEE J. Emerg. Sel. Topics Power Electron.*, vol. 9, no. 4, pp. 3971–3981, Aug. 2021.

[6] M. Salleras, M. Carmona, and S. Marco, “Issues in the use of thermal transients to achieve accurate time-constant spectrums and differential structure functions,” *IEEE Trans. Adv. Packag.*, vol. 33, no. 4, pp. 918–923, Nov. 2010.

[7] Z. Wang and W. Qiao, “An online frequency-domain junction temperature estimation method for IGBT modules,” *IEEE Trans. Power Electron.*, vol. 30, no. 9, pp. 4633–4637, Sep. 2015.

[8] C. H. van der Broeck, T. A. Polom, R. D. Lorenz, and R. W. De Doncker, “Real-time monitoring of thermal response and life-time varying parameters in power modules,” *IEEE Trans. Ind. Appl.*, vol. 56, no. 5, pp. 5279–5291, Sep./Oct. 2020.

[9] T. A. Polom, C. van der Broeck, R. W. De Doncker, and R. D. Lorenz, “Real-time, in situ degradation monitoring in power semiconductor converters,” in *Proc. IEEE Appl. Power Electron. Conf. Expo.*, 2019, pp. 2720–2727.

[10] T. A. Polom, M. Andresen, M. Liserre, and R. D. Lorenz, “Frequency-domain electrothermal impedance spectroscopy of an actively switching power semiconductor converter,” *IEEE Trans. Ind. Appl.*, vol. 55, no. 6, pp. 6161–6172, Nov./Dec. 2019.

[11] C. H. van der Broeck, S. Kalker, T. A. Polom, R. D. Lorenz, and R. W. de Doncker, “In-situ thermal impedance spectroscopy of power electronic modules for localized degradation identification,” in *Proc. PCIM Eur. Conf.*, 2019, pp. 1097–1104.

[12] J. N. Davidson, D. A. Stone, M. P. Foster, and D. T. Gladwin, “Real-time temperature estimation in a multiple device power electronics system subject to dynamic cooling,” *IEEE Trans. Power Electron.*, vol. 31, no. 4, pp. 2709–2719, Apr. 2016.

[13] K. Ma, M. Xu, and B. Liu, “Modeling and characterization of frequency-domain thermal impedance for IGBT module through heat flow information,” *IEEE Trans. Power Electron.*, vol. 36, no. 2, pp. 1330–1340, Feb. 2021.

[14] K. Ma, N. He, M. Liserre, and F. Blaabjerg, “Frequency-domain thermal modeling and characterization of power semiconductor devices,” *IEEE Trans. Power Electron.*, vol. 31, no. 10, pp. 7183–7193, Oct. 2016.

[15] G. L. Skibinski and W. A. Sethares, “Thermal parameter estimation using recursive identification,” *IEEE Trans. Power Electron.*, vol. 6, no. 2, pp. 228–239, Apr. 1991.

[16] Z. Wang and W. Qiao, “A physics-based improved cauer-type thermal equivalent circuit for IGBT modules,” *IEEE Trans. Power Electron.*, vol. 31, no. 10, pp. 6781–6786, Oct. 2016.

[17] F. N. Masana, “Thermal characterisation of power modules,” *Microelectron. Rel.*, vol. 40, no. 1, pp. 155–161, Jan. 2000.

[18] H. Cui, F. Hu, Y. Zhang, and K. Zhou, “Heat spreading path optimization of IGBT thermal network model,” *Microelectron. Rel.*, vol. 103, Dec. 2019, Art. no. 113511.

[19] F. N. Masana, “A new approach to the dynamic thermal modelling of semiconductor packages,” *Microelectron. Rel.*, vol. 41, no. 6, pp. 901–912, Jun. 2001.

[20] M. Ma et al., “A three-dimensional boundary-dependent compact thermal network model for IGBT modules in new energy vehicles,” *IEEE Trans. Ind. Electron.*, vol. 68, no. 6, pp. 5248–5258, Jun. 2021.

[21] A. S. Bahman, K. Ma, and F. Blaabjerg, “A lumped thermal model including thermal coupling and thermal boundary conditions for high-power IGBT modules,” *IEEE Trans. Power Electron.*, vol. 33, no. 3, pp. 2518–2530, Mar. 2018.

[22] *COMSOL Multiphysics Reference Manual*, Stockholm, Sweden: COMSOL , 2018.

[23] K. Ma, M. Liserre, F. Blaabjerg, and T. Kerekes, “Thermal loading and lifetime estimation for power device considering mission profiles in wind power converter,” *IEEE Trans. Power Electron.*, vol. 30, no. 2, pp. 590–602, Feb. 2015.

[24] J. Chung and G. M. Hulbert, “A time integration algorithm for structural dynamics with improved numerical dissipation: The Generalized-α method,” *J. Appl. Mech.*, vol. 60, no. 2, pp. 371–375, Jun. 1993.

[25] *Transient Dual Interface Test Method for the Measurement of the Thermal Resistance Junction to Case of Semiconductor Devices With Heat Flow Through a Single Path*. JEDEC Standard JESD51-14, 2010.

[26] *Transient thermal measurements and thermal equivalent circuit models*. Infineon Application Note AN 2015-10, 2020.

Mengqi Xu received the B.Sc. degree in electrical engineering from Nanjing University of Aeronautics and Astronautics, Nanjing, China, in 2018. He is currently working toward the Ph.D. degree in electrical engineering with Shanghai Jiao Tong University, Shanghai, China.

Her research interests include the thermal modeling and reliability analysis of power electronics.

Ke Ma (Senior Member, IEEE) received the B.Sc. and M.Sc. degrees in electrical engineering from the Zhejiang University, Hangzhou, China in 2007 and 2010 respectively, and the Ph.D. degree from the Aalborg University, Aalborg, Denmark in 2013.

He was an Assistant Professor with Aalborg University in 2014. In 2016, he was the Faculty of Shanghai Jiao Tong University, China, as a tenure-track Research Professor, and is currently the Deputy Director for Key Laboratory of Control of Power Transmission and Conversion, Ministry of Education, China. His current research interests include the power electronics and its reliability in the application of renewable energy, HVdc, and motor drive systems.

Dr. Ma is currently an Associate Editor for two IEEE Transaction journals, and Vice Chair for two IEEE Technical Committees. He was the receipient of "Excellent Young Wind Doctor Award 2014" by European Academy of Wind Energy, and several prized paper awards by IEEE.

Quan Zhong received the B.Sc. degree in electrical engineering from Wuhan University, Wuhan, China, in 2021. He is currently working toward the M.Sc. degree with Shanghai Jiao Tong University, Shanghai, China.

His research interests include health monitoring and reliability analysis of power semiconductor devices.

Marco Liserre (Fellow, IEEE) received the M.Sc. and Ph.D. degrees in electrical engineering from the Bari Polytechnic, respectively in 1998 and 2002.

He has been Associate Professor with Bari Polytechnic and since 2012, he has been a Professor in reliable power electronics with Aalborg University, Aalborg, Denmark. Since 2013, he has been a Full Professor and he holds the Chair of Power Electronics at Kiel University (Germany). He has authored or coauthored 500 technical papers (1/3 of them in international peer-reviewed journals) and a book. These works have received more than 35 000 citations. He is listed in ISI Thomson report "The world's most influential scientific minds" from 2014.

Dr. Liserre was the recipient with an ERC Consolidator Grant for the project "The Highly Efficient and Reliable smart Transformer, a new Heart for the Electric Distribution System." He is Member of IEEE Industry Applications Society, IEEE Power Electronics Society, IEEE Power and Energy Society, and IEEE Industrial Electronics Society. He has been serving all these societies in different capacities. He was also recipient of the IES 2009 Early Career Award, the IES 2011 Anthony J. Hornfeck Service Award, the 2014 Dr. Bimal Bose Energy Systems Award, the 2011 Industrial Electronics Magazine best paper award in 2011 and 2020 and the Third Prize paper award by the Industrial Power Converter Committee at ECCE 2012, 2012, 2017 IEEE PELS Sustainable Energy Systems Technical Achievement Award and the 2018 IEEE-IES Mittelmann Achievement Award.